Determination of the full elastic tensor of single crystals using shear wave velocities by Brillouin spectroscopy

DAWEI FAN[1,2,3,*], ZHU MAO[4,*], JING YANG[2] AND JUNG-FU LIN[2,3]

[1]Key Laboratory for High Temperature and High Pressure Study of the Earth's Interior, Institute of Geochemistry, Chinese Academy of Sciences, Guiyang, Guizhou 550002, China
[2]Department of Geological Sciences, Jackson School of Geosciences, The University of Texas at Austin, Austin, Texas 78712, U.S.A.
[3]Center for High Pressure Science and Technology Advanced Research (HPSTAR), Shanghai 201203, China
[4]Laboratory of Seismology and Physics of Earth's Interior, School of Earth and Space Sciences, University of Science and Technology of China, Hefei, Anhui 230026, China

ABSTRACT

Single-crystal elasticity of candidate minerals in the Earth's mantle, such as that of ferropericlase and bridgmanite, etc., is very important for understanding the seismic observations, geodynamic flow patterns, and testing geochemical and mineralogical models of the planet's deep interior. Determination of the full elastic tensor typically requires measuring both compressional and shear wave velocities (v_P and v_S) of the candidate single crystal as a function of crystallographic orientations at high pressures, but it has been a huge technical challenge obtaining v_P at pressures above 25 GPa using Brillouin light scattering coupled with in a diamond-anvil cell due to the spectral overlap of the sample v_P with the v_S of the diamond window. In this study, we present a new method to derive the full elastic tensor (C_{ij}) of single crystals using only measured v_S of a given crystal platelet as a function of the azimuthal angle. Experimentally determined v_P and v_S results from Brillouin measurements for cubic periclase (MgO) and spinel (MgAl$_2$O$_4$), tetragonal stishovite (SiO$_2$), and orthorhombic zoisite [Ca$_2$Al$_3$Si$_3$O$_{12}$(OH)] at ambient conditions are used as examples to demonstrate the application of our approach from theoretical analyses and experimental prospective. For high-symmetry cubic minerals, such as cubic MgO and spinel, a suitable crystallographic plane with small tradeoffs between any two C_{ij} in v_S is required for the method to work well such that the obtained C_{ij} using measured v_S velocities alone can be within 3% of the values derived from using both v_S and v_P. Our analyses show that the (–1,0.5,0.2) platelet for periclase and the (1,1,0) platelet for spinel are respective optimal orientations for applying our method. For lower symmetry minerals, such as tetragonal stishovite and orthorhombic zoisite, three crystallographic planes, that are orthogonal to each other and are tilted at least 20° from the principal crystallographic planes, can be used to provide reliable constraints on C_{ij} using measured v_S alone. We have extended this method to derive C_{ij} of the (–1,0.5,0.2) platelet for periclase at pressures of 5.8 and 11.3 GPa, in a high-pressure diamond-anvil cell to demonstrate the usefulness of the approach in studying the elasticity of Earth's mantle minerals at relevant pressure-temperature conditions. Our proposed approach can be extended to all other crystal systems at high pressures to overcome the constant lack of experimental v_P velocities at above 25 GPa, potentially providing new experimental and theoretical approaches in constraining the elastic tensor of the materials in the Earth's deep interior, which will be an effective strategy to solve one of the most relevant difficulties involved in the experimental study of the elastic properties (especially elastic anisotropy) of minerals of the lower mantle.

Keywords: Single-crystal elasticity, periclase, spinel, zoisite, stishovite, Brillouin light scattering

INTRODUCTION

Elastic constants (C_{ij}) describe the instantaneous reversible volume and shape changes of a mineral under stress (Birch 1952; Carpenter 2006; Bass et al. 2008; Angel et al. 2009). Determination of the full elastic tensor of a crystal of interest permits direct evaluations of several key elastic, thermodynamic, and mechanical parameters of the crystal including

adiabatic bulk modulus, shear modulus, Poisson's ratio, shear stress, shear strain, compressional wave anisotropy, and shear wave splitting anisotropy, among many others (Anderson 1989; Li et al. 2004; Sanchez-Valle et al. 2005; Mainprice 2007; Angel et al. 2009). Of particular importance to our understanding of deep-Earth mineral physics is the elasticity of minerals as a function of pressure and temperature (*P-T*) at conditions relevant to the Earth's mantle. These results can be directly compared to seismic observations of the deep Earth to constrain mineralogical and compositional models of the Earth interior, and better understand the geodynamic behavior

* E-mail: fandawei@vip.gyig.ac.cn (Dawei Fan) or zhumao@ustc.edu.cn (Zhu Mao).

of the deep Earth (e.g., Weidner and Carleton 1977; Weidner et al. 1978; Duffy and Anderson 1989; Weidner and Zhao 1992; Zha et al. 1996; Sinogeikin et al. 2003, 2004; Li et al. 2006; Li and Liebermann 2007; Bass 2008; Bass et al. 2008; Angel et al. 2009; Mao et al. 2012; Murakami et al. 2012; Lu et al. 2013; Yang et al. 2014). Specifically, the single-crystal elasticity at deep-mantle conditions is of particular importance in understanding the anisotropy and dynamic flow pattern of the deep planet (Duffy et al. 1995; Zha et al. 1998; Jacobsen et al. 2002; Sinogeikin et al. 2005; Chen et al. 2006; Jackson et al. 2007). The ability to experimentally obtain elastic constants of minerals with sufficient accuracy thus plays an indispensable role in our understanding of the Earth's deep interior.

Brillouin light scattering (BLS) coupled with a diamond-anvil cells (DAC) has been extensively used to constrain the elasticity of earth materials at high pressures and/or high temperatures (e.g., Duffy and Anderson 1989; Shimizu and Sasaki 1992; Shimizu 1995; Duffy et al. 1995; Zha et al. 1996, 1998; Sinogeikin and Bass 2000; Sinogeikin et al. 2006; Murakami et al. 2009a, 2009b; Mao et al. 2008, 2012; Lu et al. 2013; Yang et al. 2014). The frequency shifts of the BLS spectra represent a collection of inelastic scattering events arising from the interactions between incident photons of the laser and thermally excited acoustic phonons of the sample (Polian 2003). The technique permits the measurement of one longitudinal acoustic v_P and two transverse acoustic v_{S1} and v_{S2} velocities of a single crystal along a certain direction at a given scattering angle (or momentum transfer) (Sinogeikin and Bass 2000). The integration of the BLS technique with the DAC is well suited for studying the single-crystal elasticity of crystals at P-T conditions relevant to the deep interior of the planet. The majority of geophysical relevant materials of the deep interior of Earth are optically transparent minerals (Bass et al. 2008; Speziale et al. 2014), which makes it possible to use BLS to study their elastic properties to the relevant conditions of the deep Earth. However, because of the overlap of the v_P of the sample with the v_S of diamond anvils, it has been extremely difficult to measure v_P to constrain full elastic moduli of a given candidate single crystal at approximately above 25 GPa (e.g., Zha et al. 2000; Marquardt et al. 2009a, 2009b), especially for measuring v_P of bridgmanite, ferropericlase, post-bridgmanite by BLS at the relevant pressures of the lower mantle. Such a technical problem has significantly hampered our understanding of the deep-Earth physics and chemistry using experimental elasticity results. Alternative approaches have been proposed to remedy this diamond window problem, but these attempts have not been very successful at high P-T conditions (e.g., Jackson et al. 2006; Speziale et al. 2014). Examples of these studies include the use of pre-oriented diamond anvils with known orientations and velocities to reduce the overlap at certain orientations (Yang et al. 2014), the addition of a diamond wedge to reduce chromatic aberration from the diamond anvil (Zha et al. 1998, 2000), as well as the adoption of a long focusing lens to focus the laser to the sample with a small beam divergence (Zha et al. 1998, 2000; Lu et al. 2013; Speziale et al. 2014; Yang et al. 2014). Nevertheless, the diamond window issue remains one of the major technical hurdles that has prevented mineral physicists from having a better understanding of the seismic structure and

the mineralogical model of the Earth's deep interior (Zha et al. 2000; Bass 2007; Bass et al. 2008; Marquardt et al. 2009a, 2009b; Speziale et al. 2014).

Based on the expansion of the Christoffel's equation, the elastic constants of a given crystal in any given crystal system are intrinsically coupled with one another, although, depending on the crystal system, the coupling strength can vary in different directions (Every 1980). Therefore, it is theoretically possible to derive full elastic tensor of a given crystal using partial information on v_P and/or v_S data sets (Every 1980); though, this method has not yet been tested practically. In this study, we present theoretical derivations and experimental BLS results to derive full elastic tensor of a single crystal using only the v_S velocity data set as a function of the azimuthal angle for a pre-selected crystal platelet. The validity of the results was tested using derived elastic constants from both v_P and v_S results as references. Using cubic periclase and spinel as well as orthorhombic zoisite and tetragonal stishovite as examples, we show that the full elastic tensor of crystal in the cubic, tetragonal or orthorhombic systems can be well constrained using the measured v_S velocities alone. We have also derived C_{ij} of periclase with an optimal (–1,0.5,0.2) platelet at high pressure using BLS measurements in a DAC to justify the use of our method at high pressures. Being able to determine the full single-crystal elastic tensor of a mineral by using only v_S data would allow us to largely improve our constraints on the mineralogy of the deep Earth by comparing mineral physics results with seismic models. In fact, despite the constant progress both in large-scale geophysics models and in experimental and computational mineral physics, we cannot perform precise tests of proposed mineralogical models of the lowermost mantle against seismic data and models based on v_P seismic velocities. Future applications of this new method at high P-T conditions of the Earth's interior can help shed new light on single-crystal elasticity of candidate minerals relevant to the Earth's deep interior.

THEORETICAL BACKGROUND

Based on the Christoffel's equation, the sound velocity (v) of a crystal can be described by the following characteristic Equation:

$$\left| \Gamma_{ij} - \rho v^2 \delta_{ij} \right| = 0 \tag{1}$$

where ρ is the density, δ_{ij} is the Kronecker δ, and Γ_{ij} is the coefficient in the Christoffel matrix. The values of the Christoffel coefficients (Γ_{ij}) depend on the single-crystal constants (C_{ij}) in the reduced Voigt notation in which the propagation direction of the sound velocity is described by the cosines of the velocity direction, n_i. It follows that the Christoffel's equation 1 can be expanded to relate these parameters mathematically in various directions such that one can then pre-select a certain crystal plane for deriving full elastic tensor using the v_S or the v_P data set alone. Here we follow the classical paper by Every (1980) to expand Equation 1 for the cubic system below. The full expansion of the Christoffel's equation for other crystal systems can also be derived using similar derivation schemes given below and in Every (1980).

For the cubic structure, Γ_{ij} is given by:

$$\Gamma_{11} = C_{11}n_1^2 + C_{44}n_2^2 + C_{44}n_3^2$$
$$\Gamma_{22} = C_{11}n_2^2 + C_{44}n_1^2 + C_{44}n_3^2$$
$$\Gamma_{33} = C_{11}n_3^2 + C_{44}n_1^2 + C_{44}n_2^2$$
$$\Gamma_{23} = \Gamma_{32} = (C_{11} + C_{12})n_2 n_3$$
$$\Gamma_{13} = \Gamma_{31} = (C_{11} + C_{12})n_1 n_3$$
$$\Gamma_{12} = \Gamma_{21} = (C_{11} + C_{12})n_1 n_2 \qquad (2)$$

Equation 1 can be presented in a simplified form by carrying out a linear transformation that eliminates the quadratic term in the Equation 3 below as follows:

$$3\rho v^2 = T + S \qquad (3)$$

$$T = (C_{11} + 2C_{44})(n_1^2 + n_2^2 + n_3^2) \qquad (4)$$

$$\left| \Lambda_{ij} - S\delta_{ij} \right| = 0 \qquad (5)$$

$$\Lambda_{ij} = 3\Gamma_{ij} - T\delta_{ij} \qquad (6)$$

where T is the first invariant of Γ_{ij}, S is the real root of Γ_{ij}, Λ_{ij} is a function of the elastic constants and direction cosines of the wave vector. For the cubic structure, it follows that:

$$\Lambda_{11} = 3\left(C_{11}n_1^2 + C_{44}n_2^2 + C_{44}n_3^2\right) - (C_{11} + 2C_{44})(n_1^2 + n_2^2 + n_3^2)$$
$$\Lambda_{22} = 3\left(C_{11}n_2^2 + C_{44}n_1^2 + C_{44}n_3^2\right) - (C_{11} + 2C_{44})(n_1^2 + n_2^2 + n_3^2)$$
$$\Lambda_{33} = 3\left(C_{11}n_3^2 + C_{44}n_1^2 + C_{44}n_2^2\right) - (C_{11} + 2C_{44})(n_1^2 + n_2^2 + n_3^2) \quad (7)$$
$$\Lambda_{23} = \Lambda_{32} = 3n_2 n_3 (C_{12} + C_{44})$$
$$\Lambda_{13} = \Lambda_{31} = 3n_1 n_3 (C_{12} + C_{44})$$
$$\Lambda_{12} = \Lambda_{21} = 3n_1 n_2 (C_{12} + C_{44})$$

Expansion of the determinant in the Equation 5 allows the derivation of the following cubic form for S:

$$S^3 - 3GS - 2H = 0 \qquad (8)$$

where G and H are the second and third invariants of Λ_{ij}. Rearranging the Equation 8, the triple root of the cubic form (S_k) is represented as:

$$S_k = 2G^{\frac{1}{2}}\cos\left(\psi + \frac{2}{3}\pi k\right) \qquad (k = 0,1,2) \qquad (9)$$

where k is the polarization index, which is only related to the absolute value of the solutions. $k = 0$ always corresponds to the fastest velocity, while $k = 1$ corresponds to the second intermediate, and $k = 2$ to the slowest velocity, and

$$\psi = \frac{1}{3}\arccos\left(H / G^{\frac{3}{2}}\right) \qquad (10)$$

Based on the Equation 5, variables G and H are given as:

$$H = \frac{|\Lambda|}{2} = \frac{(\Lambda_{11}\Lambda_{22}\Lambda_{33} + 2\Lambda_{12}\Lambda_{23}\Lambda_{31} - \Lambda_{11}\Lambda_{23}^2 - \Lambda_{22}\Lambda_{31}^2 - \Lambda_{33}\Lambda_{12}^2)}{2}$$
$$= (C_{11} - C_{44})^3 (n_1^6 + n_2^6 + n_3^6) - \frac{9}{2}(C_{11} - C_{12} - 2C_{44})(C_{11} - C_{44})(C_{11} + C_{12}) \quad (11)$$

$$3\rho v_k^2 = (C_{11} + 2C_{44})(n_1^2 + n_2^2 + n_3^2) + 2G^{1/2}\cos\left(\frac{1}{3}\arccos(H / G^{\frac{3}{2}})\right) + \frac{2}{3}\pi k \qquad (12)$$

It follows that the velocity of a cubic crystal along a given direction (v_k) as shown in the Equation 3 can be expressed in terms of the three elastic constants (C_{11}, C_{12}, C_{44}):

$$3\rho v_{S1}^2 = (C_{11} + 2C_{44})(n_1^2 + n_2^2 + n_3^2) + 2G^{1/2}\cos\left(\frac{1}{3}\arccos(H / G^{\frac{3}{2}}) + \frac{2}{3}\pi\right) \qquad (13)$$

We note that although the off-diagonal C_{12} elastic constant is not shown explicitly in the Equation 13, it has been represented in the H and G terms (see Eqs. 11 and 12 for details). With experimentally determined C_{ij}, one can thus derive the velocities of a cubic crystal along specific directions of the crystal using Equations 11, 12, and 13. Inversely, the full elastic tensor of a cubic crystal can be derived numerically from a set of measured velocities along various crystallographic orientations using the non-linear least-squares Levenberg-Marquardt method (Press 1988). This method has been widely used to derive the full C_{ij} of minerals and materials from high-pressure BLS measurements in the last few decades (e.g., Duffy et al. 1995; Zha et al. 1996).

The aforementioned method has the advantage of resolving full elastic tensor using available v_S velocities from Brillouin measurements. Derivations of the longitudinal elastic constant (C_{11}) typically require having the v_P of the crystal, but the longitudinal acoustic peaks in the BLS spectra normally overlap with the v_S peaks of the diamond anvils at pressures above 25 GPa. Such a problem with the spectral overlap is prevalent in most oxide and silicate minerals of the deep Earth, such as bridgmanite and ferropericlase, when studied in a DAC (e.g., Marquardt et al. 2009a, 2009b; Speziale et al. 2014; Zha et al. 2000). Although the constants C_{44} and C_{12} can be well constrained by measuring the v_S velocities along the principal crystallographic directions (<100>, <110>, and/or <111>) using BLS measurements, these constants from Brillouin measurements have been combined with equation of state (EoS) results from X-ray diffraction to evaluate the full elastic tensor of the crystal, especially for the longitudinal modulus (Marquardt et al. 2009a). The use of the bulk modulus (K) derived from the EoS measurements, however, greatly increases the uncertainties of the derived elastic constants, therefore reducing their reliability.

Based on our derivations of the equations above, we note that the v_S of a given crystal along certain directions also carry the necessary information to retrieve the longitudinal modulus. When v_S velocities of the crystal are the only available data set in high-pressure BLS measurements, the Equation 13 can be re-written as

$$3\rho v_{S2}^2 = (C_{11} + 2C_{44})(n_1^2 + n_2^2 + n_3^2) + 2G^{1/2}\cos\left(\frac{1}{3}\arccos(H / G^{\frac{3}{2}}) + \frac{4}{3}\pi\right) \qquad (14)$$

where v_{S1} and v_{S2} are two shear-wave velocities with polarizations orthogonal to each other, and v_{S1} is defined as having a velocity smaller than v_{S2}. To provide the necessary constraints on the longitudinal moduli C_{11} and off-diagonal moduli C_{12} by only using v_S, one must find a crystal plane with the least tradeoffs

between any two C_{ij}. We describe the procedure for determining a suitable crystal plane and deriving reliable elastic constants in the following steps:

Step 1. With known C_{ij}, density, and the Eulerian angles (θ, φ, χ), which relate the laboratory coordinate system to the crystal coordinate system (Shimizu 1995), one can predict a set of velocities along various crystallographic orientations of a mineral by following the Equation 13.

Step 2. Considering that there are always experimental errors involved in velocity measurements in BLS experiments, an error of 2% for the velocity data sets along various crystal orientations can be expected for the initial evaluations. Using this data set of velocities along various crystal orientations, one can obtain C_{ij} using the v_S velocities alone and then compare the derived elastic constants with literature results derived from using both v_P and v_S velocities.

Step 3. If one cannot obtain C_{ij} using the v_S velocities alone, one can rotate the plane by 5°, and then repeat Step 1 and Step 2 until a suitable crystal plane with minimal tradeoff coefficients for the derived elastic constants is found.

We note that the ideal planes with the least tradeoff in the C_{ij} of periclase and spinel, which both are cubic in structure and belong to the same crystal class $m\bar{3}m$, are different, due to their different elastic anisotropies. It is worth noting that the main purpose of the proposed method is to derive full elastic tensor by using only v_S velocities of a single crystal because of the constant lack of experimental v_P velocities at above 25 GPa in the BLS measurements. In this case, full elastic C_{ij}, density, and the Eulerian angles of the given crystal at ambient conditions need to be known in advance to find the ideal crystal plane for further high-pressure studies. Based on the elasticity theory (Every 1980), our study can also be expanded in the future such that the use of partial sets of velocity results (v_P, v_S, or v_P and v_S) from random lattice planes can also help researchers to evaluate full elastic tensor; however, these require further experimental tests and theoretical elaboration in the future, and are not within the scope of this article at this point in time.

For crystals in symmetries lower than the cubic system, such as zoisite in the orthorhombic system and stishovite in the tetragonal system, we found that the general method of deriving the full elastic tensor from v_S velocities is to use crystal planes that are orthogonal to each other but are at least 20° off the principal planes. We should note that the v_S in these systems can be described by an equation similar to the Equation 14, but the complexity of the equation would require the knowledge of the full elastic tensor of the crystal to derive such a plane. For example, the C_{ij} of the orthorhombic zoisite (Mao et al. 2007) exhibit the least tradeoffs in (−0.24,−0.60,0.76), (0.10,0.78,0.62), and (−0.95,0.10,−0.28) planes. In this case, any three crystal planes, which are orthogonal to each other and are at an angle at least 20° away from the principal planes (Every 1980; Mao et al. 2007), can be used to constrain all C_{ij} using v_S data set alone.

SAMPLES AND EXPERIMENTAL PROCEDURES

Single-crystal platelets of periclase (MgO) in (100), (110), and (111) crystallographic orientations and spinel (MgAl$_2$O$_4$) in (100) and (110) orientations were purchased from MTI Corporation. Based on the aforementioned numerical analyses of the least tradeoffs between C_{ij}, we have pre-oriented a periclase platelet in (−1,0.5,0.2) crystallographic orientation for testing the optimal derivations of the C_{ij}. The orientations of the crystals were determined using the single-crystal

X-ray diffractometer at the Texas Materials Institute of The University of Texas at Austin (UT-Austin). All sample platelets were doubled-side polished with two parallel surfaces using 3M diamond lapping films with a final finishing particle size of 0.5 μm. A short symmetric DAC with a large optical opening was conveniently used to hold the sample platelet with dimensions typically of 200–300 μm and thickness of 50–70 μm. No pressure was applied to the crystals in the DAC for experiments at ambient conditions.

The BLS measurements were conducted at the Mineral Physics Laboratory of UT-Austin (Lu et al. 2013; Yang et al. 2014). The Brillouin signals were excited by a Coherent Verdi V2 laser with a 532 nm wavelength and collected by a photomultiplier tube (PMT) at a low dark count rate (<2 counts/s) through a JRS six-pass tandem Fabry-Pérot Interferometer. The laser beam was focused down to approximately 20 μm in diameter at the sample position. The scattering angle of 49.6(±0.02)° for the system was calibrated using previously reported elastic constants of silicate glass (Polian et al. 2002), distilled water (Ostwald et al. 1977), and single-crystal MgO (Sinogeikin and Bass 2000).

The scattered laser light in the BLS measurements consists of an elastically scattered component with frequency, ω, as well as inelastically scattered components that have undergone a frequency shift, Δω, due to the interaction of the incident laser with thermally generated phonons in the sample crystal. In a symmetric scattering geometry, the acoustic velocity, v is calculated from the relation:

$$v = \Delta\omega\lambda/2 \sin(\theta/2) \qquad (15)$$

where λ is the incident wavelength and θ is the scattering angle. Our BLS spectra were collected from a given direction of a crystal plane and were repeated by rotating the crystal platelet 5° about the axis perpendicular to the plane at every step in a total of 37 directions. For each spectrum, the average collection time was approximately 30 min. The measured Brillouin spectra are of excellent quality with a high signal-to-noise ratio (Fig. 1). All the measured spectra display symmetric spectral pairs corresponding to the v_P and v_S modes of the sample (Fig. 1). Two v_S modes and one v_P mode were observed in most of the directions, although some Brillouin spectra only showed v_P and one v_S mode (Figs. 1–5). Further information about the BLS technique and data analyses can be found elsewhere in previous literatures (e.g., Mao et al. 2012; Lu et al. 2013; Yang et al. 2014).

DETERMINATION OF FULL ELASTIC TENSOR

Cubic periclase and spinel crystals

Brillouin measurements were obtained from six platelets [periclase in (−1,0.5,0.2), (100), (110), and (111) crystallographic orientations and spinel in (100) and (110) crystallographic orientations] over an azimuthal range of 180° with an angular increment of 5° per step (Figs. 1–4) (see Tables 1–2 and Supplementary Tables 1–4[1]). The measured acoustic velocities show a systematic dependence as a function of the orientation indicating that the velocities of periclase and spinel are directionally anisotropic (Figs. 2–4). The measured v_P and v_S velocities were modeled to derive the elastic constants using the Christoffel's equations (Eq. 1) via the best fits to both v_P and v_S velocities (Fig. 1; Fig. 4a and 4b) as well as v_S velocities alone (Fig. 2; Figs. 4c and 4d; Fig. 5).

In periclase and spinel, both cubic, C_{ij} exhibit the least tradeoff coefficients in the (−1,0.5,0.2) plane for periclase and are very close to the (110) plane for spinel (Table 3). The tradeoff coefficients corresponding to a particular i and k represent the change in an elastic constant C_i for a unit change in another elastic constant C_k. Such tradeoff coefficients are formally captured by the variance-covariance matrix for the C_{ij} and depend on the observations of v_S speed as functions of propagation directions. The approach we identified here is to find optical crystallographic planes of a given crystal with the least tradeoff in the C_{ij} at ambi-

ent conditions. In this method, the C_{ij} at ambient conditions need to be known in advance to find the ideal crystal plane, and then the full elastic moduli of the ideal crystal plane can be derived by using the measured v_S velocities alone at high pressure. The derivation of the full elastic tensor can be extended beyond this method by conducting iterations in the derived elastic constants using v_S or v_P data sets alone via minimization of the misfits. The derived values of tradeoff coefficients are very small and thus indicate that all of the elastic constants are well resolved within the context of the linear relation. The above inversion scheme indicates that the interdependence of the elastic constants of periclase in the $(-1,0.5,0.2)$ plane and spinel in the (110) plane are applicable and thus suggest that the v_S data set can be used to uniquely and reliably constrain all of the elastic constants.

We have used a nonlinear inversion procedure to solve the Christoffel's equations for the three independent single-crystal elastic constants (C_{ij}) of the cubic periclase and spinel; this non-linear inversion procedure uses the Gauss-Newton algorithm with Levenberg-Marquardt modifications for global convergence of the solutions, and has been widely adopted for finding solutions to the Christoffel's equations (Weidner and Carleton 1977; Sanchez-Valle et al. 2005). The elastic constants of the periclase and spinel obtained in this work are listed in Tables 4–5, together with previous results for comparison. Within experimental uncertainties, our results derived from using both v_P and v_S profiles for periclase in $(-1,0.5,0.2)$, (100), (110), and (111) orientations and for spinel in (110) and (100) orientations

are in excellent agreement with those obtained from previous measurements (Tables 4 and 5) (Jackson and Niesler 1982; Yoneda 1990; Askarpour et al. 1993; Sinogeikin and Bass 2000; Zha et al. 2000; Suzuki et al. 2000). Furthermore, the derived elastic constants of periclase using the v_S data set alone for each (100), (110), or (111) crystallographic orientation deviate from the results derived from using both v_P and v_S data sets as well as literature Brillouin results (Jackson and Niesler 1982; Yoneda 1990; Sinogeikin and Bass 2000; Zha et al. 2000) (Figs. 6–7 and Table 4), especially for C_{11} and C_{12}. For example, the difference can reach to approximately 70% for C_{12} and 25% for C_{11} between $(-1,0.5,0.2)$ and (111) orientations (Fig. 7a). In contrast, the C_{11}, C_{12}, and C_{44} constants for periclase derived from using the v_S profiles alone in the $(-1,0.5,0.2)$ orientation are 296.7 (± 1.3), 99.6 (± 1.5), 155.0 (± 0.2) GPa, respectively, and are consistent with the literature values (Jackson and Niesler 1982; Yoneda 1990; Sinogeikin and Bass 2000; Zha et al. 2000) (Fig. 6a; Table 4). In addition, the estimated uncertainties of the derived value for the longitudinal moduli C_{11}, shear moduli C_{44}, and off-diagonal moduli C_{12} in the pre-selected $(-1,0.5,0.2)$ crystallographic orientation is better than 1.6% (1σ level), while the estimated uncertainties are approximately 42% in the (100), (110), and (111) crystallographic orientation. Likewise, the C_{11}, C_{12}, and C_{44} of the cubic spinel derived from using the v_S profiles alone in the (100) crystallographic orientation are noticeably different from the values derived from using both v_P and v_S data sets and from previous literature values (Table 5) with the maximum
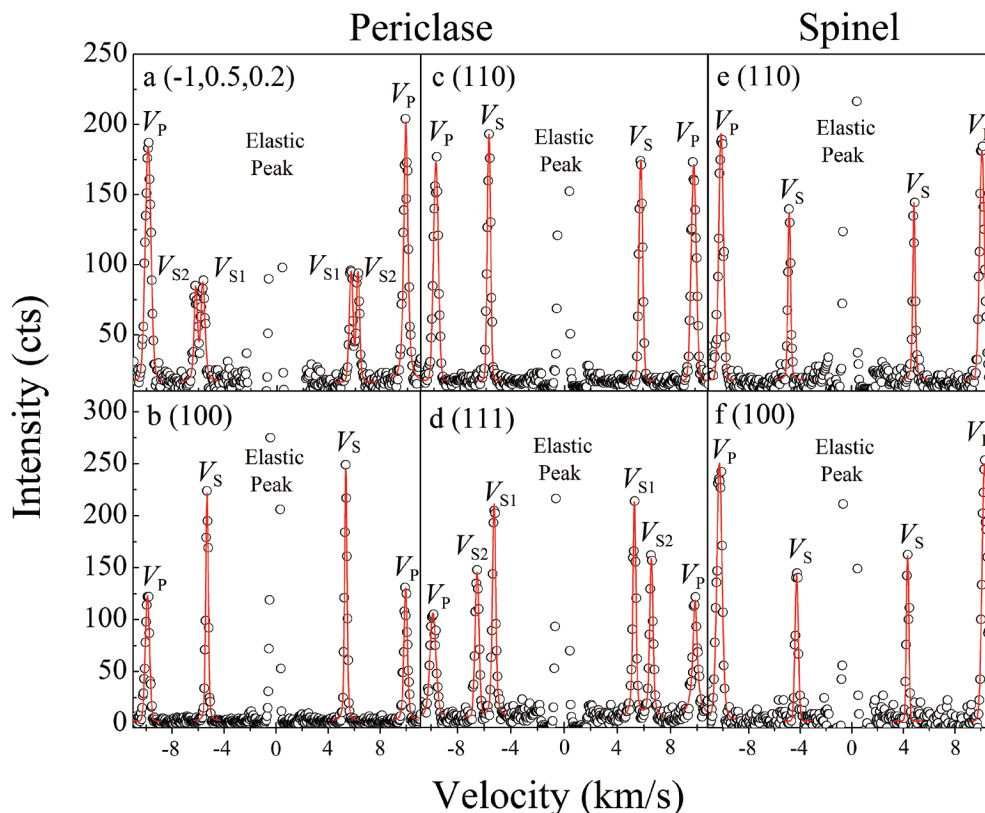

FIGURE 1. Representative Brillouin spectra of the single-crystal periclase and spinel at ambient conditions. The orientation of each crystal platelet is labeled on the corresponding spectrum. Open circles = experimental data; solid lines = fitted v_P and v_S peaks. (Color online.)
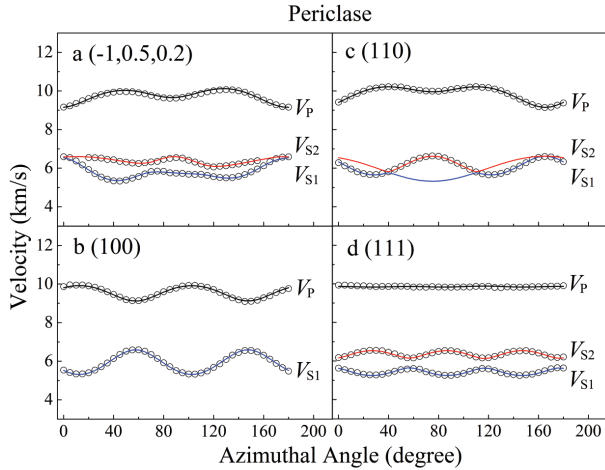
FIGURE 2. Acoustic v_P and v_S velocities of the single-crystal periclase as a function of the azimuthal angle in four representative crystallographic planes. (**a**) (–1,0.5,0.2); (**b**) (100); (**c**) (110); (**d**) (111). Open circles = experimental data; solid lines = modeled fits for deriving C_{ij} from using both v_P and v_S. (Color online.)
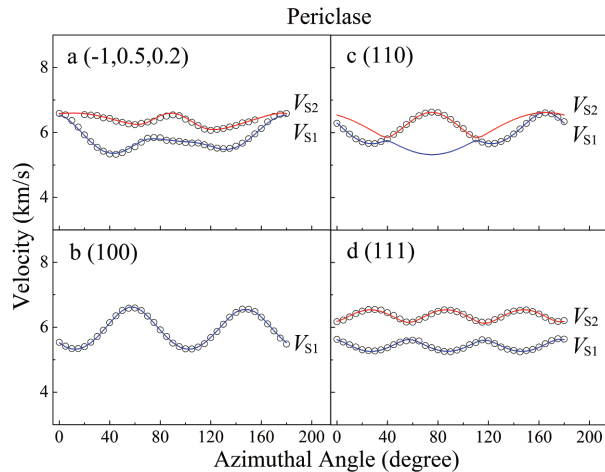

FIGURE 4. Acoustic v_P and v_S velocities of the single-crystal spinel as a function of the azimuthal angle in two representative crystallographic planes. (**a** and **b**) Measured and modeled velocities for deriving C_{ij} using both v_P and v_S. (**c** and **d**) Measured and modeled velocities for deriving C_{ij} using v_S velocities alone. Open circles = experimental data; solid lines = modeled fits. (Color online.)

FIGURE 3. Acoustic v_S velocities of the single-crystal periclase as a function of the azimuthal angle in four representative crystallographic planes. The velocities are the same as shown in Figure 2, but the full elastic tensor were derived from the modeled fits (solid lines) using experimentally measured v_S velocities alone (open circles). (Color online.)

FIGURE 5. Acoustic v_S velocities of the single-crystal zoisite as a function of the azimuthal angle in three representative crystallographic planes. Open circles = experimental data (Mao et al. 2007); solid lines = modeled fits for deriving C_{ij} using v_S velocities alone. (Color online.)

difference reaching approximately 30% for C_{12} and 15% for C_{11} between (110) and (100) orientations (Fig. 7b). The derived elastic constants of the cubic spinel are: C_{11} = 291.3 (±1.2), C_{12} = 152.6 (±1.2), and C_{44} = 155.7 (±0.4) GPa in the pre-selected (110) orientation determined from using the v_S data set alone, which are consistent with the literature values (Yoneda 1990; Askarpour et al. 1993; Suzuki et al. 2000) (Fig. 6b; Table 5). We should note that the estimated uncertainties of the derived value for these constants is better than 0.8% (1σ level) in the (110) platelet, while the estimated uncertainties is better than 5% in the (100) platelet.

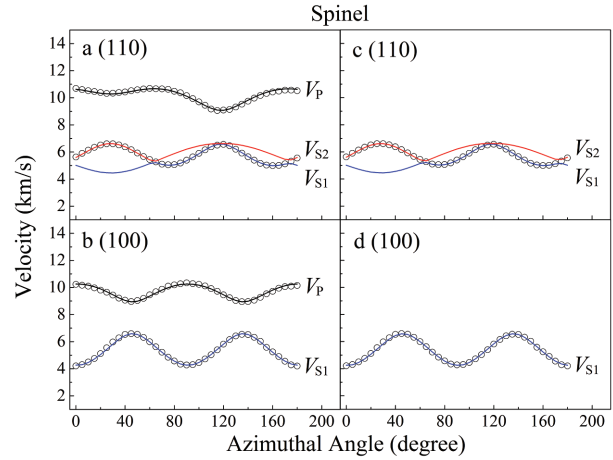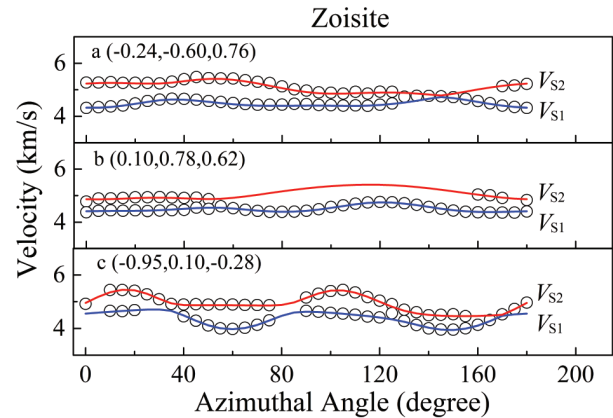Based on the aforementioned experimental analyses, the

derived elastic constants from the pre-selected (–1,0.5,0.2) orientation for periclase and (110) orientation for spinel validate the theoretical derivations for obtaining the full single-crystal elastic constants using the v_S data set alone. Since our proposed methodology for deriving full elastic tensor is based on modeling v_S as a function of the azimuthal angle for a given crystal platelet, we have also tested the sensitivity of the method on the measuring intervals of the v_S values. Comparisons between the values derived from 5° and 10° measuring intervals show that the elastic constants derived from the 10° interval measurements slightly deviate from the 5° interval counterparts and previous literature results by 8% and 7%, respectively (Fig. 8; Table 6). The deviation is most significant for C_{11} at 8% and C_{12} at 7% (Fig. 8; Table 6). We thus conclude that having at least a 5° measuring interval for the v_S data set is needed to reliably derive the elastic constants of the cubic crystal.

Orthorhombic zoisite and tetragonal stishovite

The application of the method can be extended beyond simple cubic crystals as shown above. Here we have used previously reported Brillouin results for orthorhombic zoisite (space group: *Pnma*) and tetragonal stishovite (space group: $P4_2/mnm$) as two representative examples to extend the applications of our methodology. The elastic tensor of orthorhombic crystals has nine independent coefficients that can be used to completely describe its elastic properties (Zha et al. 1996; Sanchez-Valle et al. 2005; Jackson et al. 2007; Mao et al. 2007, 2010). To determine all elastic constants of an orthorhombic crystal such as zoisite, three mutually perpendicular platelets are desirable for sound velocity measurements (Sanchez-Valle et al. 2005; Jackson et al. 2007; Mao et al. 2007). Using the v_S data set alone, the velocity data for all planes in BLS measurements were simultaneously fitted to Christoffel's equation (Every 1980). The procedure to retrieve the elastic constants has been discussed elsewhere in details (Mao et al. 2007). Analyses of the measured and calculated best-fit velocities of zoisite at ambient conditions indicate excellent agreements among the velocities (Fig. 5).

Three platelets orthogonal to each other but otherwise randomly oriented were used to obtain the full elastic tensor of orthorhombic zoisite, and we also found that the C_{ij} of zoisite exhibit

very small tradeoffs in (−0.24,−0.60,0.76), (0.10,0.78,0.62), and (−0.95,0.10,−0.28) planes. Comparisons between the elastic constants of zoisite using both the v_P and v_S data sets and the v_S data set alone in the pre-selected crystallographic planes show that most of the elastic constants for zoisite in the pre-selected crystallographic planes are reasonably consistent within experimental uncertainties, except for the off-diagonal modulus C_{23} (Table 7). The estimated uncertainties of the derived values is better than 2.6% (1σ level) for all other elastic constants, but the estimated uncertainties for the C_{23} is approximately 11.4%. The relatively large difference of 17% for C_{23} is mainly due to the much smaller value of the C_{23} compared to other elastic constants; the derived value of the C_{23} is 27.5 GPa, which is among the smallest of all elastic constants of zoisite, and 11.4% estimated uncertainties translates into a value of 22.8 GPa for its elastic constant. We should note that this difference in the C_{23} constant is still acceptable when compared with other elastic constants of zoisite. In fact, the value of C_{23} determined using the v_S data set alone is completely comparable to the value determined by using both v_P and v_S data sets within experimental uncertainties, justifying the use of the v_S data set alone to retrieve full elastic tensor of zoisite.

One can also extend the application of this new approach to other crystal systems. For example, stishovite crystallizes in the

TABLE 1. Measured acoustic v_P and v_S velocities of the single-crystal periclase (MgO) as a function of the crystallographic orientation within the (−1,0.5,0.2) plane at ambient conditions

Azimuthal angle (degree)	v_P (km/s)	v_{S1} (km/s)	v_{S2} (km/s)
0	9.276 (±0.004)	6.538 (±0.010)	
5	9.302 (±0.005)	6.472 (±0.007)	
10	9.393 (±0.006)	6.327 (±0.008)	
15	9.489 (±0.008)	6.165 (±0.005)	
20	9.600 (±0.009)	5.926 (±0.005)	6.542 (±0.008)
25	9.735 (±0.007)	5.714 (±0.004)	6.532 (±0.006)
30	9.806 (±0.007)	5.541 (±0.003)	6.471 (±0.008)
35	9.880 (±0.009)	5.422 (±0.004)	6.426 (±0.011)
40	9.931 (±0.008)	5.338 (±0.006)	6.402 (±0.009)
45	9.966 (±0.014)	5.326 (±0.006)	6.343 (±0.007)
50	9.956 (±0.012)	5.378 (±0.011)	6.301 (±0.005)
55	9.929 (±0.011)	5.476 (±0.008)	6.267 (±0.005)
60	9.855 (±0.008)	5.562 (±0.007)	6.241 (±0.006)
65	9.759 (±0.005)	5.681 (±0.007)	6.277 (±0.004)
70	9.694 (±0.005)	5.749 (±0.009)	6.320 (±0.007)
75	9.614 (±0.005)	5.763 (±0.014)	6.371 (±0.009)
80	9.549 (±0.005)	5.753 (±0.013)	6.453 (±0.011)
85	9.537 (±0.008)	5.727 (±0.006)	6.535 (±0.011)
90	9.524 (±0.006)	5.706 (±0.012)	6.540 (±0.008)
95	9.588 (±0.005)	5.696 (±0.006)	6.506 (±0.008)
100	9.676 (±0.006)	5.686 (±0.005)	6.412 (±0.006)
105	9.760 (±0.007)	5.674 (±0.010)	6.314 (±0.007)
110	9.869 (±0.005)	5.636 (±0.007)	6.212 (±0.007)
115	9.952 (±0.005)	5.603 (±0.004)	6.104 (±0.006)
120	10.007 (±0.013)	5.555 (±0.005)	6.064 (±0.006)
125	10.044 (±0.010)	5.517 (±0.004)	6.095 (±0.007)
130	10.065 (±0.012)	5.481 (±0.003)	6.124 (±0.006)
135	10.055 (±0.008)	5.484 (±0.003)	6.169 (±0.010)
140	10.004 (±0.013)	5.558 (±0.005)	6.214 (±0.006)
145	9.930 (±0.006)	5.668 (±0.004)	6.284 (±0.007)
150	9.838 (±0.006)	5.804 (±0.005)	6.315 (±0.008)
155	9.713 (±0.005)	5.955 (±0.005)	6.376 (±0.006)
160	9.576 (±0.006)	6.121 (±0.009)	
165	9.462 (±0.006)	6.326 (±0.009)	
170	9.368 (±0.006)	6.455 (±0.010)	
175	9.299 (±0.006)	6.523 (±0.010)	
180	9.291 (±0.007)	6.554 (±0.010)	

Notes: The azimuthal angle is expressed as the rotated angle with respect to an arbitrary reference direction within the plane. Numbers in parentheses are standard deviations (±1σ).

TABLE 2. Measured acoustic v_P and v_S velocities of the single-crystal spinel (MgAl$_2$O$_4$) as a function of the crystallographic orientation within the (110) plane at ambient conditions

Azimuthal angle (degree)	v_P (km/s)	v_S (km/s)
0	10.681 (±0.004)	5.637 (±0.003)
5	10.605 (±0.006)	5.896 (±0.003)
10	10.522 (±0.004)	6.137 (±0.002)
15	10.464 (±0.002)	6.353 (±0.003)
20	10.393 (±0.003)	6.513 (±0.002)
25	10.329 (±0.003)	6.606 (±0.002)
30	10.348 (±0.004)	6.609 (±0.002)
35	10.390 (±0.002)	6.524 (±0.002)
40	10.437 (±0.006)	6.375 (±0.002)
45	10.523 (±0.003)	6.169 (±0.003)
50	10.599 (±0.002)	5.918 (±0.002)
55	10.659 (±0.002)	5.666 (±0.003)
60	10.688 (±0.004)	5.440 (±0.004)
65	10.686 (±0.005)	5.274 (±0.005)
70	10.656 (±0.002)	5.096 (±0.003)
75	10.628 (±0.008)	5.067 (±0.005)
80	10.481 (±0.008)	5.077 (±0.004)
85	10.373 (±0.009)	5.182 (±0.004)
90	10.165 (±0.005)	5.390 (±0.008)
95	9.933 (±0.008)	5.643 (±0.006)
100	9.703 (±0.008)	5.902 (±0.007)
105	9.455 (±0.011)	6.168 (±0.007)
110	9.178 (±0.009)	6.388 (±0.006)
115	9.062 (±0.007)	6.512 (±0.005)
120	9.093 (±0.008)	6.557 (±0.005)
125	9.149 (±0.006)	6.459 (±0.007)
130	9.325 (±0.004)	6.208 (±0.004)
135	9.533 (±0.006)	5.921 (±0.006)
140	9.739 (±0.005)	5.650 (±0.006)
145	9.987 (±0.007)	5.399 (±0.005)
150	10.175 (±0.005)	5.168 (±0.006)
155	10.328 (±0.006)	5.035 (±0.005)
160	10.440 (±0.006)	4.991 (±0.005)
165	10.519 (±0.009)	5.011 (±0.006)
170	10.575 (±0.008)	5.138 (±0.006)
175	10.586 (±0.014)	5.323 (±0.005)
180	10.561 (±0.009)	5.549 (±0.005)

Notes: The azimuthal angle is expressed as the rotated angle with respect to an arbitrary reference direction within the plane. Numbers in parentheses are standard deviations (±1σ).

TABLE 3. Trade-off coefficients for elastic constants of single-crystal periclase (MgO) within (–1,0.5,0.2) plane and spinel (MgAl$_2$O$_4$) within (110) plane

	$k\rightarrow$		
$i\downarrow$	11	12	44
	periclase		
11	0.044147	0.001501	–0.000149
12	0.001501	0.013785	–0.002397
44	–0.000149	–0.002397	0.018163
	spinel		
11	0.014740	0.004580	–0.002577
12	0.004580	0.019508	–0.005696
44	–0.002577	–0.005696	0.088773

TABLE 4. Single-crystal elastic constants of periclase (MgO) at ambient conditions

Orientation and References	Data used	C_{11} (GPa)	C_{12} (GPa)	C_{44} (GPa)
(–1,0.5,0.2) This study	v_P and v_S	296.0 (±0.4)	96.8 (±0.4)	154.6 (±0.2)
	v_S	296.7 (±1.3)	99.6 (±1.5)	155.0 (±0.2)
(100) This study	v_P and v_S	297.5 (±0.3)	95.2 (±0.3)	155.6 (±0.2)
	v_S	271 (±16)	69 (±16)	157.2 (±0.6)
(110) This study	v_P and v_S	298.6 (±0.5)	96.8 (±0.4)	156.5 (±0.2)
	v_S	246 (±7)	42 (±8)	157.3 (±0.2)
(111) This study	v_P and v_S	296.6 (±0.4)	94.7 (±0.4)	154.8 (±0.2)
	v_S	229 (±13)	31 (±13)	153.3 (±0.2)
(100) Jackson and Niesler (1982)	v_P and v_S	296.8 (±1.5)	95.3 (±0.2)	155.8 (±0.2)
(100) Yoneda (1990)	v_P and v_S	297.8 (±1.5)	95.1 (±1.0)	155.8 (±1.5)
(100) Sinogeikin and Bass (2000)	v_P and v_S	297.9 (±1.5)	95.8 (±1.0)	154.4 (±2.0)
(01$\bar{1}$) Zha et al. (2000)	v_P and v_S	297.0 (±0.1)	95.2 (±0.7)	155.7 (±0.5)

Notes: Numbers in parentheses are standard deviations (±1σ). Literature results are also listed for comparison.

TABLE 5. Single-crystal elastic constants of spinel (MgAl$_2$O$_4$) at ambient conditions

Orientation and References	Data used	C_{11} (GPa)	C_{12} (GPa)	C_{44} (GPa)
(110) This study	v_P and v_S	288.0 (±0.5)	154.2 (±0.5)	156.2 (±0.3)
	v_S	291.3 (±1.2)	152.6 (±1.2)	155.7 (±0.4)
(100) This study	v_P and v_S	284.4 (±0.3)	155.0 (±0.4)	154.7 (±0.2)
	v_S	321 (±9)	193 (±9)	153.9 (±0.3)
(110) Yoneda (1990)	v_P and v_S	282.9[a]	155.4[a]	154.8[a]
(100) Askarpour et al. (1993)	v_P and v_S	286.3 (±5.3)	157.2 (±3.4)	153.5 (±2.7)
Suzuki et al. (2000)[b]	v_P and v_S	281.3 (±0.1)	155.4 (±0.1)	154.6 (±0.1)

Notes: Numbers in parentheses are standard deviations (±1σ). Literature results are also listed for comparison.
[a] Uncertainties of the elastic constants were not given in the literature.
[b] The orientation of the sample in Suzuki et al. (2000) is not specified because the elastic tensor was determined by resonant ultrasound spectroscopy performed on a spherical sample.

tetragonal system (space group: $P4_2/mnm$) with six independent non-zero elastic constants: C_{11}, C_{12}, C_{13}, C_{33}, C_{44}, and C_{66} (Weidner et al. 1982; Jiang et al. 2009). The elastic constants of stishovite were measured previously at ambient conditions using Brillouin spectroscopy (Weidner et al. 1982; Brazhkin et al. 2005). Recently, Jiang et al. (2009) also conducted acoustic velocities measurements on three crystal platelets of single-crystal stishovite in a forward symmetric scattering geometry using Brillouin spectroscopy; these experimental results permitted them to retrieve full elastic tensor of the sample at ambient conditions (Table 8). Here we have used the reported v_S data set for the crystal planes of stishovite by Jiang et al. (2009) to derive full elastic tensor using the Christoffel's equation (Every 1980) (Table 8). Comparisons between the elastic constants of stishovite using both v_P and v_S data sets and the v_S data set alone show that all of the elastic constants for stishovite

are reasonably consistent within experimental uncertainties (Table 8). The estimated uncertainties of the derived values are better than 1.9% (1σ level) for all of the elastic constants. The relatively large difference of 4.0% for C_{12} and 8.3% for C_{13} mainly comes from the much smaller value of each constant, respectively, as compared to other elastic constants (the value of C_{13} is among the smallest constants for all elastic constants of stishovite). It should be noted that the difference in the C_{12} and C_{13} constant is still acceptable when compared with other elastic constants of stishovite
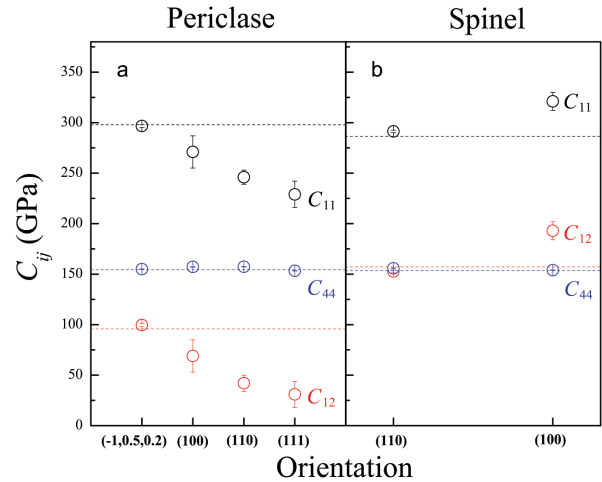

FIGURE 6. Derived elastic constants of the single-crystal periclase and spinel in the representative crystallographic planes at ambient conditions. These constants and their uncertainties were derived using the experimentally measured v_S velocities alone. The (–1,0.5,0.2) plane for periclase and (110) plane for spinel show the smallest uncertainties (±1σ) and mismatches from the reference elastic constants taken from the literatures (dash line) for periclase (Sinogeikin and Bass 2000) and for spinel (Askarpour et al. 1993). (**a**) (–1,0.5,0.2) plane for periclase; (**b**) (110) plane for spinel. (Color online.)
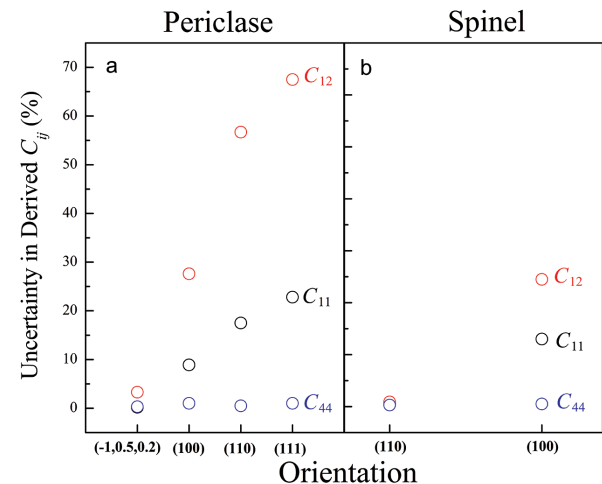

FIGURE 7. Uncertainties in the derived C_{ij} for single-crystal periclase and spinel using v_S profiles as well as both v_P and v_S profiles in the representative crystallographic planes at ambient conditions. The (–1,0.5,0.2) plane for periclase and (110) plane for spinel show the smallest uncertainties (±1σ). (**a**) Periclase; (**b**) spinel. (Color online.)
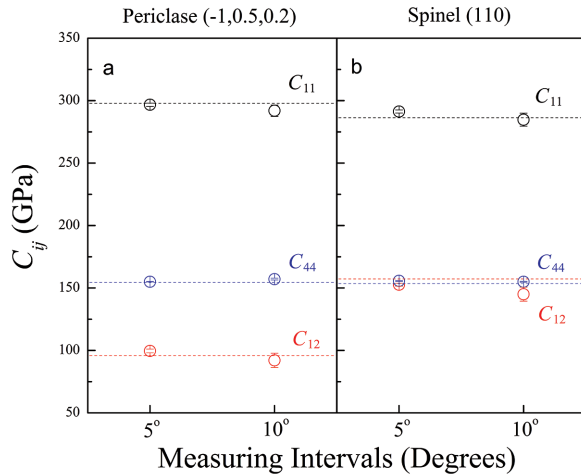
FIGURE 8. Derived elastic constants of the single-crystal periclase and spinel using 5° and 10° measuring interval at ambient conditions. The measuring interval was determined from the rotation angle of the crystal platelet on the rotatory stage. The (−1,0.5,0.2) plane for periclase and (110) plane for spinel were used for the study, and the elastic constants and their uncertainties were derived using the v_S velocities alone. The data set with a 5° measuring interval shows very small uncertainties (±1σ) and mismatches to the reference literature values (dash line) (Sinogeikin and Bass 2000; Askarpour et al. 1993). (**a**) (−1,0.5,0.2) plane for periclase; (**b**) (110) plane for spinel. (Color online.)

and that the value of C_{12} and C_{13} determined by v_S profile alone is also entirely comparable to the value determined by both v_P and v_S profiles within experimental uncertainties. These analyses highlight the application of deriving full elastic tensor from using v_S data sets alone for other tetragonal crystals.

TABLE 6. Single-crystal elastic constants of periclase (MgO) and spinel (MgAl$_2$O$_4$) derived using the v_S velocities alone data set having 5° and 10° measuring intervals at ambient conditions

Sample and Orientation	Interval	Data used	C_{11} (GPa)	C_{12} (GPa)	C_{44} (GPa)
Periclase (−1,0.5,0.2)	5°	v_S	296.7 (±1.3)	99.6 (±1.5)	155.0 (±0.2)
	10°	v_S	291.9 (±4.6)	92.0 (±5.7)	157.1 (±0.7)
Spinel (110)	5°	v_S	291.3 (±1.2)	152.6 (±1.2)	155.7 (±0.4)
	10°	v_S	284.7 (±5.2)	145.0 (±5.6)	155.0 (±0.4)

Note: Numbers in parentheses are standard deviations (±1σ).

TABLE 7. Single-crystal elastic constants of zoisite [Ca$_2$Al$_3$Si$_3$O$_{12}$(OH)] at ambient conditions

Modulus	Data used[a] v_P and v_S	Data used[a] v_S	Difference %
C_{11} (GPa)	279.8 (±0.6)	276.8 (±1.7)	1.1
C_{12} (GPa)	94.7 (±1.1)	90.1 (±2.3)	4.9
C_{13} (GPa)	88.7 (±1.0)	85.2 (±1.4)	3.9
C_{22} (GPa)	249.2 (±0.6)	243.4 (±0.8)	2.3
C_{23} (GPa)	27.5 (±0.7)	22.8 (±2.6)	17.2
C_{33} (GPa)	209.4 (±0.9)	205.5 (±3.2)	1.8
C_{44} (GPa)	51.8 (±0.3)	51.8 (±0.2)	0.1
C_{55} (GPa)	81.4 (±0.3)	81.6 (±0.4)	0.2
C_{66} (GPa)	66.3 (±0.3)	66.2 (±0.5)	0.1

Notes: The difference in percentage is calculated as the difference between the elastic constants of zoisite using v_P and v_S velocities and v_S velocities alone using Mao et al. (2007) as the reference. Numbers in parentheses are standard deviations (±1σ).
[a] Data were taken from Mao et al. (2007).

DISCUSSION

There have previously proposed methods to solve the problem in which the Brillouin scattering signal corresponding to compressional velocities of samples was masked at pressures above 25 GPa (Zha et al. 2000; Marquardt et al. 2009a, 2009b). Marquardt et al. (2009a, 2009b) reported that in the case of cubic structure materials, in situ X-ray diffraction data can be used to supplement the Brillouin scattering data at pressures above 25 GPa where the BLS signals corresponding to v_P was masked. Using the adiabatic bulk modulus, $K_S = (C_{11} + 2C_{12})/3$, together with the v_S results from Brillouin scattering, they had extracted the C_{11}, C_{12}, and C_{44} of a cubic ferropericlase up to 81 GPa (Marquardt et al. 2009a). However, the method used by Marquardt et al. (2009a, 2009b) is more suitable for cubic structure materials and is not as useful for crystals with lower symmetries. In addition, Zha et al. (1998, 2000) also introduced a method that utilized a spatial filter and cylindrical lenses to suppress the diamond signal (Zha et al. 1998, 2000) such that the v_P signal at relatively higher pressures of approximately above 25 GPa can be detected. It still remains difficult to apply this method to materials with very fast v_P as well as to other lower symmetry systems. Thus far, deriving reliable C_{ij} at high pressures remains challenging. Our proposed approach overcomes these difficulties and has the advantage of being suitable for deriving reliable elastic constants for all crystal systems at high pressures.

To test the usefulness of our method at high pressures, we have conducted high-pressure BLS measurements on the pre-selected (−1,0.5,0.2) platelet of cubic periclase as a function of the azimuthal angles at 5.8(4) and 11.3(5) GPa, respectively. The sample platelet was loaded into a DAC containing Ne gas as pressure-transmitting medium and ruby spheres as the pressure calibrant (Mao et al. 1986). At each pressure, Brillouin spectra were collected in 37 directions over an angular range of 180° with a 5° step. Since deriving full elastic tensor requires knowledge of the sample's density, we have used the equation of state of the MgO and have followed a nonlinear inversion procedure proposed previously in Speziale and Duffy (2002) to determine the density at each given pressure.

Individual C_{ij} values for the cubic periclase are obtained from fitting the measured velocities using Christoffel's equation (Table 9). The derived elastic constants of the cubic periclase using the v_S data set alone are: $C_{11} = 352.8$ (±3.6), $C_{12} = 107.7$ (±3.2), $C_{44} = 165.1$ (±2.8) GPa at 5.8(4) GPa and $C_{11} = 399.4$ (±4.4), $C_{12} = 113.3$ (±3.7), $C_{44} = 171.1$ (±3.8) GPa at 11.3(5) GPa, which are very consistent with the results from using both v_P and v_S pro-

TABLE 8. Single-crystal elastic constants of stishovite (SiO$_2$) at ambient conditions

Modulus	Data used[a] v_P and v_S	Data used[a] v_S	Difference %
C_{11} (GPa)	455 (±1)	447 (±4)	1.8
C_{12} (GPa)	199 (±2)	207 (±4)	4.0
C_{13} (GPa)	192 (±1)	208 (±3)	8.3
C_{33} (GPa)	762 (±1)	755 (±3)	0.9
C_{44} (GPa)	258 (±1)	260 (±4)	0.8
C_{66} (GPa)	321 (±1)	319 (±5)	0.6

Notes: The difference in percentage is calculated as the difference between the elastic constants of stishovite using v_P and v_S velocities and v_S velocities alone using Jiang et al. (2009) as the reference. Numbers in parentheses are standard deviations (±1σ).
[a] Data were taken from Jiang et al. (2009).

files [C_{11} = 348.0 (±2.8), C_{12} = 103.1 (±2.5), C_{44} = 162.6 (±2.4) GPa at 5.8(4) GPa and C_{11} = 394.8 (±3.8), C_{12} = 109.1 (±3.1), C_{44} = 168.5 (±2.4) GPa at 11.3(5) GPa] within experimental uncertainties (Fig. 9). The derived individual C_{ij} values for the cubic periclase at 5.8(4) GPa and 11.3(5) GPa in this study are also very consistent with literature values at similar pressures of 5.5(1) and 11.00(2) GPa, respectively (Sinogeikin and Bass 2000) (Fig. 9; Table 9). As shown in Figure 9 and Table 9, the derived elastic constants of the cubic periclase from the pre-selected (–1,0.5,0.2) orientation using the v_S data set alone are in agreement well with previous Brillouin scattering measurements within their uncertainties, supporting our proposed approach of using the pre-selected crystallographic orientation to derive full elastic tensor at high pressures. We should also note that our proposed method can also be combined with the partially available v_P data set at high pressure to help constrain the elastic tensors. The derivation of the elastic constants from the v_S data set alone using multiple platelets with different orientations for a given crystal can also help resolve the elastic constants with less uncertainty.

IMPLICATIONS

Future applications of our proposed approach can have significant implications especially on understanding seismic structures, geochemistry, and mineralogy of the Earth's lower mantle with pressures ranging from 23 to 136 GPa and temperatures from approximately 1800 to 3500 K, at which conditions the traditional BLS approach has had some limitations (e.g., Zha et al. 2000; Marquardt et al. 2009a, 2009b; Speziale et al. 2014). Recently, Brillouin scattering spectroscopy has been coupled with a laser-heated DAC to measure v_S of the Earth's lower mantle minerals up to lowermost-mantle pressures (Murakami et al. 2012). After comparison with seismic profiles of the lower mantle, these v_S results have suggested a perovskitic lower-mantle composition, although v_P profiles of the candidate minerals were not available for the comparison (Murakami et al. 2012). Thus far, the determination of the chemical composition of the Earth's lower mantle remains challenging due to the limitation of the elasticity data mentioned above (e.g., Ringwood 1975; Sun 1982; Anderson 1989; Ito and Takahashi 1989; Allègre et al. 1995; Fiquet et al. 2000; Murakami et al. 2004, 2012; Lin et al. 2013). Accurate knowledge of sound velocities and elastic properties in the Earth's lower mantle minerals, namely ferro-periclase and bridgmanite, under relevant high P-T conditions can thus provide essential constraints on the mineralogy and chemical compositions of the region (e.g., Oganov et al. 2001; Sinogeikin et al. 2004; Jackson et al. 2005, 2006; Crowhurst et al. 2008; Reichmann et al. 2008; Marquardt et al. 2009a, 2009b; Chen et al. 2012; Murakami et al. 2012).

Particularly, the elasticity of single-crystal ferropericlase $(Mg_{0.9}Fe_{0.1})O$ has been studied recently using Brillouin scattering and X-ray diffraction up to 81 GPa in the DAC (Marquardt et al. 2009a). It has been shown that the spin crossover of ferrous iron is accompanied by the v_P and C_{11} softening, but the BLS measurements with only v_S values available do not provide direct information in deciphering this softening phenomena because of the overlap of the Brillouin signal with the v_S peaks of the diamond anvils in the DAC (Marquardt et al. 2009b). Our

TABLE 9. Single-crystal elastic constants of periclase (MgO) at high pressures

Orientation and References	Pressure (GPa)	Data used	C_{11} (GPa)	C_{12} (GPa)	C_{44} (GPa)
(–1,0.5,0.2) This study	5.8 (±0.4)	v_P and v_S	348.0 (±2.8)	103.1 (±2.5)	162.6 (±2.4)
		v_S	352.8 (±3.6)	107.7 (±3.2)	165.1 (±2.8)
	11.3 (±0.5)	v_P and v_S	394.8 (±3.8)	109.1 (±3.1)	168.5 (±2.4)
		v_S	399.4 (±4.4)	113.3 (±3.7)	171.1 (±3.8)
(100) Sinogeikin	5.5 (±0.1)	v_P and v_S	346.9 (±3.0)	102.0 (±2.0)	158.4 (±2.0)
and Bass (2000)	11.00 (±0.02)	v_P and v_S	390.4 (±3.0)	110.1 (±3.0)	165.2 (±3.0)

Notes: Literature results from Sinogeikin and Bass (2000) are also listed for comparison. Numbers in parentheses are standard deviations (±1σ).
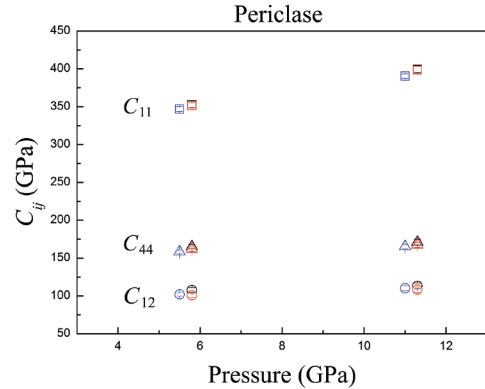

FIGURE 9. Derived elastic constants of the single-crystal periclase at high pressure. These constants and their uncertainties were derived from the representative crystallographic (–1,0.5,0.2) plane using the experimentally measured v_S velocities alone. The black symbols with error bars are the present data points, the blue and red symbols with error bars are the reference elastic constants taken from Sinogeikin and Bass (2000) and Zha et al. (2000), respectively. Open squares = C_{11}; open triangles = C_{44}; open circles = C_{12}. (Color online.)

proposed approach can overcome the spectral limitation of the Brillouin scattering and can be applied to investigate the effects of the spin transition on the elasticity of lower-mantle ferro-periclase at relevant P-T conditions (Wentzcovitch et al. 2009; Wu et al. 2013). Furthermore, our approach can also be used to investigate the elasticity of bridgmanite [Al-bearing silicate perovskite Al-$(Mg,Fe)SiO_3$], the most abundant mineral phase in Earth's lower mantle. It is somewhat surprising to note that the single-crystal elasticity of bridgmanite has only been determined at ambient conditions using BLS (Yeganeh-Haeri et al. 1989; Yeganeh-Haeri 1994; Jackson et al. 2004; Sinogeikin et al. 2004), while high-pressure single-crystal elasticity of bridgmanite has not yet been reported (Speziale et al. 2014). Thus far, the v_P and v_S of polycrystalline Fe-free bridgmanite has been reported at pressures up to 25 GPa (Jackson et al. 2005; Murakami et al. 2007; Chantel et al. 2012), and its v_S has been investigated over the entire P-T range of the lower mantle (Murakami et al. 2007). The lack of the single-crystal elastic constants for bridgmanite at relevant P-T conditions has limited our ability to accurately model the mineralogy and seismic anisotropy of the Earth's lower mantle. In addition, the potential effect of the electronic spin transition of iron on the elastic properties of bridgmanite is still unknown (Lin et al. 2013). Application of our new approach in studying the elasticity of single-crystal bridgmanite at high P-T will quantify its elastic anisotropy. Our approach can also be used

to calculate its aggregate v_P and v_S, and to assess the effect of the electronic spin transition of iron on the elastic properties of bridgmanite. Therefore, this approach can significantly enhance our understanding of the Earth's lower mantle seismology and composition (Murakami et al. 2007; Speziale et al. 2014).

References cited

Allègre, C.J., Poirier, J.P., Humler, E., and Hofmann, A.W. (1995) The chemical compositions of the Earth. Earth and Planetary Science Letters, 134, 515–526.
Anderson, D.L. (1989) Theory of the Earth. Blackwell, Boston.
Angel, R.J., Jackson, J.M., Reichmann, H.J., and Speziale, S. (2009) Elasticity measurements on minerals: A review. European Journal of Mineralogy, 21, 525–550.
Askarpour, V., Manghnani, M.H., Fassbender, S., and Yoneda, A. (1993) Elasticity of single-crystal MgAl$_2$O$_4$ spinel up to 1273 K by Brillouin spectroscopy. Physics and Chemistry of Minerals, 19, 511–519.
Bass, J.D. (2007) Theory and practice—Techniques for measuring high P/T elasticity. In G.D. Price, Ed., Treatise on Geophysics-Mineral Physics, 2, p. 269–291. Elsevier, Amsterdam.
——— (2008) Recent progress in studies of the elastic properties of earth materials. Physics of the Earth and Planetary Interiors, 170, 207–209.
Bass, J.D., Sinogeikin, S.V., and Li, B.S. (2008) Elastic properties of minerals: A key for understanding the composition and temperature of Earth's interior. Elements, 4, 165–170.
Birch, F. (1952) Elasticity and constitution of the Earth's interior. Journal of Geophysical Research, 57, 227–286.
Brazhkin, V.V., McNeil, L.E., Grimsditch, M., Bendeliani, N.A., Dyuzheva, T.I., and Lityagina, L.M. (2005) Elastic constants of stishovite up to its amorphization temperature. Journal of Physics: Condensed Matter, 17, 1869–1875.
Carpenter, M.A. (2006) Elastic properties of minerals and the influence of phase transitions. American Mineralogist, 91, 229–246.
Chantel, J., Frost, D.J., McCammon, C.A., Jing, Z.C., and Wang, Y.B. (2012) Acoustic velocities of pure and iron-bearing magnesium silicate perovskite measured to 25 GPa and 1200 K. Geophysical Research Letters, 39, L19307.
Chen, B., Jackson, J.M., Sturhahn, W., Zhang, D.Z., Zhao, J.Y., Wicks, J.K., and Murphy, C.A. (2012) Spin crossover equation of state and sound velocities of (Mg$_{0.65}$Fe$_{0.35}$)O ferropericlase to 140 GPa. Journal of Geophysical Research, 117, B08208.
Chen, P.F., Chiao, L.Y., Huang, P.H., Yang, Y.J., and Liu, L.G. (2006) Elasticity of magnesite and dolomite from a genetic algorithm for inverting Brillouin spectroscopy measurements. Physics of the Earth and Planetary Interiors, 155, 73–86.
Crowhurst, J.C., Brown, J.M., Goncharov, A.F., and Jacobsen, S.D. (2008) Elasticity of (Mg,Fe)O through the spin transition of iron in the lower mantle. Science, 319, 451–453.
Duffy, T.S., and Anderson, D.L. (1989) Seismic velocities in mantle minerals and the mineralogy of the upper mantle. Journal of Geophysical Research, 94, 1895–1912.
Duffy, T.S., Zha, C.S., Downs, R.T., Mao, H.K., and Hemley, R.J. (1995) Elasticity of forsterite to 16 GPa and the composition of the upper-mantle. Nature, 378, 170–173.
Every, A.G. (1980) General closed-form expressing for acoustic waves in elastically anisotropic solids. Physical Review B, 22, 1746–1760.
Fiquet, G., Dewaele, A., Andrault, D., Kunz, M., and Le Bihan, M. (2000) Thermoelastic properties and crystal structure of MgSiO$_3$ perovskite at lower mantle pressure and temperature conditions. Geophysical Research Letters, 27, 21–24.
Ito, E., and Takahashi, E. (1989) Postspinel transformations in the system Mg$_2$SiO$_4$-Fe$_2$SiO$_4$ and some geophysical implications. Journal of Geophysical Research, 94, 10637–10646.
Jackson, I., and Niesler, H. (1982) The elasticity of periclase to 3 GPa and some geophysical implications. In S. Akimoto and M.H. Manghnani, Eds., High Pressure Research in Geophysics, p. 93–113. Center for Academic Publishing, Tokyo, Japan.
Jackson, J.M., Zhang, J.Z., and Bass, J.D. (2004) Sound velocities and elasticity of aluminous MgSiO$_3$ perovskite: Implications for aluminum heterogeneity in Earth's lower mantle. Geophysical Research Letters, 31, L10614.
Jackson, J.M., Zhang, J.Z., Shu, J.F., Sinogeikin, S.V., and Bass, J.D. (2005) High-pressure sound velocities and elasticity of aluminous MgSiO$_3$ perovskite to 45 GPa: Implications for lateral heterogeneity in Earth's lower mantle. Geophysical Research Letters, 32, L21305.
Jackson, J.M., Sinogeikin, S.V., Jacobsen, S.D., Reichmann, H.J., Mackwell, S.J., and Bass, J.D. (2006) Single-crystal elasticity and sound velocities of (Mg$_{0.94}$Fe$_{0.06}$)O ferropericlase to 20 GPa. Journal of Geophysical Research, 111, B09203.
Jackson, J.M., Sinogeikin, S.V., and Bass, J.D. (2007) Sound velocities and single-crystal elasticity of orthoenstatite to 1073K at ambient pressure. Physics of the Earth and Planetary Interiors, 161, 1–12.
Jacobsen, S.D., Reichmann, H.J., Spetzler, H.A., Mackwell, S.J., Smyth, J.R., Angel, R.J., and McCammon, C.A. (2002) Structure and elasticity of single-crystal (Mg,Fe)O and a new method of generating shear waves for gigahertz ultrasonic interferometry. Journal of Geophysical Research, 107, http://dx.doi.org/10.1029/2001JB000490.
Jiang, F.M., Gwanmesia, G.D., Dyuzheva, T.I., and Duffy, T.S. (2009) Elasticity of stishovite and acoustic mode softening under high pressure by Brillouin scattering. Physics of the Earth and Planetary Interiors, 172, 235–240.
Li, B.S., and Liebermann, R.C. (2007) Indoor seismology by probing the Earth's interior by using sound velocity measurements at high pressures and temperatures. Proceedings of the National Academy of Sciences, 104, 9145–9150.
Li, B.S., Kung, J., and Liebermann, R.C. (2004) Modern techniques in measuring elasticity of Earth materials at high pressure and high temperature using ultrasonic interferometry in conjunction with synchrotron X-radiation in multi-anvil apparatus. Physics of the Earth and Planetary Interiors, 143–144, 559–574.
Li, L., Weidner, D.J., Brodholt, J., Alfe, D., and Price, D.G. (2006) Elasticity of Mg$_2$SiO$_4$ ringwoodite at mantle conditions. Physics of the Earth and Planetary Interiors, 157, 181–187.
Lin, J.F., Speziale, S., Mao, Z., and Marquardt, H. (2013) Effects of the electronic spin transitions of iron in lower-mantle minerals: Implications for deep-mantle geophysics and geochemistry. Reviews of Geophysics, 51, 244–275.
Lu, C., Mao, Z., Lin, J.F., Zhuravlev, K.K., Tkachev, S.N., and Prakapenka, V.B. (2013) Elasticity of single-crystal iron-bearing pyrope up to 20 GPa and 750 K. Earth and Planetary Science Letters, 361, 134–142.
Mainprice, D. (2007) Seismic anisotropy of the deep Earth from a mineral and rock physics perspective. Treatise on Geophysics, 2, 437–491.
Mao, H.K., Xu, J., and Bell, P.M. (1986) Calibration of the ruby pressure gauge to 800 kbar under quasi-hydrostatic conditions. Journal of Geophysical Research, 91, 4673–4676.
Mao, Z., Jiang, F.M., and Duffy, T.S. (2007) Single-crystal elasticity of zoisite Ca$_2$Al$_3$Si$_3$O$_{12}$(OH) by Brillouin scattering. American Mineralogist, 92, 570–576.
Mao, Z., Jacobsen, S.D., Jiang, F., Smyth, J.R., Holl, C.M., and Duffy, T.S. (2008) Elasticity of hydrous wadsleyite to 12 GPa: Implications for Earth's transition zone. Geophysical Research Letters, 35, L21305.
Mao, Z., Jacobsen, S.D., Jiang, F., Smyth, J.R., Holl, C.M., Frost, D.J., and Duffy, T.S. (2010) Velocity crossover between hydrous and anhydrous forsterite at high pressures. Earth and Planetary Science Letters, 293, 250–258.
Mao, Z., Lin, J.F., Jacobsen, S.D., Duffy, T.S., Chang, Y.Y., Smyth, J.R., Frost, D.J., Hauri, E.H., and Prakapenka, V.B. (2012) Sound velocities of hydrous ringwoodite to 16GPa and 673K. Earth and Planetary Science Letters, 331, 112–119.
Marquardt, H., Speziale, S., Reichmann, H.J., Frost, D.J., and Schilling, F.R. (2009a) Single-crystal elasticity of (Mg$_{0.9}$Fe$_{0.1}$)O to 81 GPa. Earth and Planetary Science Letters, 287, 345–352.
Marquardt, H., Speziale, S., Reichmann, H.J., Frost, D.J., Schilling, F.R., and Garnero, E.J. (2009b) Elastic shear anisotropy of ferropericlase in Earth's lower mantle. Science, 324, 224–226.
Murakami, M., Hirose, K., Kawamura, K., Sata, N., and Ohishi, Y. (2004) Postperovskite phase transition in MgSiO$_3$. Science, 304, 855–858.
Murakami, M., Sinogeikin, S.V., Hellwig, H., Bass, J.D., and Li, J. (2007) Sound velocity of MgSiO$_3$ perovskite to Mbar pressure. Earth and Planetary Science Letters, 256, 47–54.
Murakami, M., Asahara, Y., Ohishi, Y., Hirao, N., and Hirose, K. (2009a) Development of in situ Brillouin spectroscopy at high pressure and high temperature with synchrotron radiation and infrared laser heating system: Application to the Earth's deep interior. Physics of the Earth and Planetary Interiors, 174, 282–291.
Murakami, M., Ohishi, Y., Hirao, N., and Hirose, K. (2009b) Elasticity of MgO to 130 GPa: Implications for lower mantle mineralogy. Earth and Planetary Science Letters, 277, 123–129.
Murakami, M., Ohishi, Y., Hirao, N., and Hirose, K. (2012) A perovskite lower

mantle inferred from high-pressure, high-temperature sound velocity data. Nature, 485, 90–94.

Oganov, A.R., Brodholt, J.P., and Price, G.D. (2001) The elastic constants of $MgSiO_3$ perovskite at pressures and temperatures of the Earth's mantle. Nature, 411, 934–937.

Ostwald, J., Pazold, W., and Weis, O. (1977) High-resolution Brillouin spectroscopy of water. Applied Physics, 13, 351–356.

Polian, A. (2003) Brillouin scattering at high pressure: An overview. Journal of Raman Spectroscopy, 34, 633–637.

Polian, A., Vo-Thanh, D., and Richet, P. (2002) Elastic properties of a-SiO_2 up to 2300 K from Brillouin scattering measurements. Europhysics Letters, 57, 375–381.

Press, W.H. (1988) Numerical recipes in C: The art of scientific computing, XXII, 735 p. Cambridge University Press, U.K.

Reichmann, H.J., Sinogeikin, S.V., and Bass, J.D. (2008) Single-crystal elastic properties of $(Mg_{0.987},Fe_{0.013})O$ to 9 GPa. American Mineralogist, 93, 1306–1311.

Ringwood, A.E. (1975) Composition and Petrology of the Earth's Mantle. McGraw Hill, New York.

Sanchez-Valle, C., Sinogeikin, S.V., Lethbridge, Z.A.D., Walton, R.I., Smith, C.W., Evans, K.E., and Bass, J.D. (2005) Brillouin scattering study on the single-crystal elastic properties of natrolite and analcime zeolites. Journal of Applied Physics, 98, 053508.

Shimizu, H. (1995) High-pressure Brillouin scattering of molecular single-crystals grown in a diamond-anvil cell. In M. Senoo, K. Suito, T. Kobayashi, and H. Kubota, Eds., High Pressure Research on Solids, pp. 1–17. Elsevier, Amsterdam.

Shimizu, H., and Sasaki, S. (1992) High-pressure Brillouin studies and elastic properties of single-crystal H_2S grown in a diamond cell. Science, 257, 514–516.

Sinogeikin, S.V., and Bass, J.D. (2000) Single-crystal elasticity of pyrope and MgO to 20 GPa by Brillouin scattering in the diamond cell. Physics of the Earth and Planetary Interiors, 120, 43–62.

Sinogeikin, S.V., Bass, J.D., and Katsura, T. (2003) Single-crystal elasticity of ringwoodite to high pressures and high temperatures: implications for 520 km seismic discontinuity. Physics of the Earth and Planetary Interiors, 136, 41–66.

Sinogeikin, S.V., Zhang, J.Z., and Bass, J.D. (2004) Elasticity of single crystal and polycrystalline $MgSiO_3$ perovskite by Brillouin spectroscopy. Geophysical Research Letters, 31, L06620.

Sinogeikin, S.V., Lakshtanov, D.L., Nicholas, J.D., Jackson, J.M., and Bass, J.D. (2005) High temperature elasticity measurements on oxides by Brillouin spectroscopy with resistive and IR laser heating. Journal of the European Ceramic Society, 25, 1313–1324.

Sinogeikin, S.V., Bass, J.D., Prakapenka, V.B., Lakshtanov, D., Shen, G.Y., Sanchez-Valle, C., and Rivers, M. (2006) Brillouin spectrometer interfaced with synchrotron radiation for simultaneous X-ray density and acoustic velocity measurements. Review of Scientific Instruments, 77, 103905.

Speziale, S., and Duffy, T.S. (2002) Single-crystal elastic constants of fluorite (CaF_2) to 9.3 GPa. Physics and Chemistry of Minerals, 29, 465–472.

Speziale, S., Marquardt, H., and Duffy, T.S. (2014) Brillouin scattering and its application in geosciences. Reviews in Mineralogy and Geochemistry, 78, 543–603.

Sun, S.S. (1982) Chemical-composition and origin of the Earth's primitive mantle. Geochimica et Cosmochimica Acta, 46, 179–192.

Suzuki, I., Ohno, I., and Anderson, O. (2000) Harmonic and anharmonic properties of spinel $MgAl_2O_4$. American Mineralogist, 85, 304–311.

Weidner, D.J., and Carleton, H.R. (1977) Elasticity of coesite. Journal of Geophysical Research, 82, 1334–1346.

Weidner, D.J., and Zhao, Y. (1992) Elasticity and equation of state of perovskite: implications for the Earth's lower mantle. Geophysical Monograph, 67, 191–196.

Weidner, D.J., Wang, H., and Ito, J. (1978) Elasticity of orthoenstatite. Physics of the Earth and Planetary Interiors, 17, P7–P13.

Weidner, D.J., Bass, J.D., Ringwood, A.E., and Sinclair, W. (1982) The single-crystal elastic moduli of stishovite. Journal of Geophysical Research, 87, 4740–4746.

Wentzcovitch, R.M., Justo, J.F., Wu, Z.Q., da Silva, C.R.S., Yuen, D.A., and Kohlstedt, D. (2009) Anomalous compressibility of ferropericlase throughout the iron spin crossover. Proceedings of the National Academy of Sciences, 106, 8447–8452.

Wu, Z.Q., Justo, J.F., and Wentzcovitch, R.M. (2013) Elastic anomalies in a spin-crossover system: Ferropericlase at lower mantle condition. Physical Review Letters, 110, 228501.

Yang, J., Mao, Z., Lin, J.F., and Prakapenka, V.B. (2014) Single-crystal elasticity of the deep-mantle magnesite at high pressure and temperature. Earth and Planetary Science Letters, 392, 292–299.

Yeganeh-Haeri, A. (1994) Synthesis and re-investigation of the elastic properties of single-crystal magnesium silicate perovskite. Physics of the Earth and Planetary Interiors, 87, 111–121.

Yeganeh-Haeri, A., Weidner, D.J., and Ito, E. (1989) Elasticity of $MgSiO_3$ in the perovskite strucutre. Science, 243, 787–789.

Yoneda, A. (1990) Pressure derivatives of elastic constants of single crystal MgO and $MgAl_2O_4$. Journal of the Physics of the Earth, 38, 19–55.

Zha, C.S., Duffy, T.S., Downs, R.T., and Hemley, R.J. (1996) Sound velocity and elasticity of single-crystal forsterite to 16 GPa. Journal of Geophysical Research, 101, 17,535–17,545.

Zha, C.S., Duffy, T.S., Downs, R.T., Mao, H.K., and Hemley, R.J. (1998) Brillouin scattering and X-ray diffraction of San Carlos olivine: Direct pressure determination to 32 GPa. Earth and Planetary Science Letters, 159, 25–33.

Zha, C.S., Mao, H.K., and Hemley, R.J. (2000) Elasticity of MgO and a primary pressure scale to 55 GPa. Proceedings of the National Academy of Sciences, 97, 13,494–13,499.